JOURNAL OF GEOPHYSICAL RESEARCH, VOL. 114, E11004, doi:10.1029/2009JE003406, 2009

Radar remote sensing of pyroclastic deposits in the southern Mare Serenitatis and Mare Vaporum regions of the Moon

Lynn M. Carter,[1] Bruce A. Campbell,[1] B. Ray Hawke,[2] Donald B. Campbell,[3] and Michael C. Nolan[4]

Received 21 April 2009; revised 12 July 2009; accepted 3 August 2009; published 5 November 2009.

[1] We use polarimetric radar observations to study the distribution, depth, and embedded rock abundance of nearside lunar pyroclastic deposits. Radar images were obtained for Mare Vaporum and the southern half of Mare Serenitatis; the imaged areas contain the large Rima Bode, Mare Vaporum, Sulpicius Gallus, and Taurus-Littrow pyroclastic deposits. Potential pyroclastic deposits at Rima Hyginus crater, the Tacquet Formation, and a dome in Mare Vaporum are also included. Data were acquired at S band (12.6 cm wavelength) using Arecibo Observatory and the Green Bank Telescope in a bistatic configuration. The S band images have resolutions between 20 and 100 m/pixel. The pyroclastic deposits appear dark to the radar and have low circular polarization ratios at S band wavelengths because they are smooth, easily penetrable by radar waves, and generally contain few embedded blocks. Changes in circular polarization ratio (CPR) across some of the pyroclastic deposits show areas with increased rock abundance as well as deposits that are shallower. Radar backscatter and CPR maps are used to identify fine-grained mantling deposits in cases where optical and near-infrared data are ambiguous about the presence of pyroclastics. The Tacquet Formation in southern Serenitatis, areas near Hyginus crater, and a dome in Mare Vaporum have lower-backscatter cross sections than would be expected for mare basalts of similar estimated titanium content. Combined with very low CPR values, this is strong evidence that these areas are covered in fine-grained pyroclastic mantling material.

Citation: Carter, L. M., B. A. Campbell, B. R. Hawke, D. B. Campbell, and M. C. Nolan (2009), Radar remote sensing of pyroclastic deposits in the southern Mare Serenitatis and Mare Vaporum regions of the Moon, *J. Geophys. Res.*, *114*, E11004, doi:10.1029/2009JE003406.

1. Introduction

[2] Pyroclastic deposits record the early history of volcanism on the Moon and contain mineral resources (metal oxides and volatiles) of potential future use. There are over 100 mapped pyroclastic deposits on the Moon, ranging in size from a few km^2 to 49,000 km^2 [*Gaddis et al.*, 2003]. At both optical and radar wavelengths, they are low-albedo features, typically associated with mare boundaries, centers of volcanism within the mare, and floor fractures in impact craters [e.g., *Gaddis et al.*, 2003; *Zisk et al.*, 1974]. The optically dark, fine-grained deposits usually appear to drape over or mantle the underlying terrain. The thinner deposits fill in local depressions and leave high topography uncovered [*Gaddis et al.*, 1985; *Lucchitta and Schmidt*, 1974]. In some cases, the source of the volcanism is evident, as is the case for the large deposit near Aristarchus that has a cobra head source area with a rille that cuts across the plateau [e.g., *Gaddis et al.*, 2003; *Campbell et al.*, 2008]. In other instances, no source region has been identified.

[3] The very large (over 2500 km^2) pyroclastic deposits, such as those in the Aristarchus, Taurus-Littrow, Sulpicius Gallus, Rima Bode and Vaporum regions, are thought to have formed from long-duration fire fountaining accompanying basaltic volcanism, but the small pyroclastic deposits were probably emplaced through episodic volcanic events [*Weitz et al.*, 1998; *Hawke et al.*, 1989; *Wilson and Head*, 1981]. Age dating of material found at the Apollo 17 site shows that the pyroclastics were formed 3.48–3.66 Ga [*Tera and Wasserburg*, 1976]. Many of the pyroclastic deposits are associated with late Imbrian aged impact craters or volcanics, suggesting that they formed around 3.2 to 3.7 Ga [*Adams et al.*, 1974; *Gaddis et al.*, 2003].

[4] The composition of lunar pyroclastics has been studied using telescopic and spacecraft remote sensing spectroscopy and though laboratory analysis of Apollo samples. Large pyroclastic deposits, such as Taurus-Littrow, Aristarchus and Sulpicius Gallus contain Fe^{2+}-bearing volcanic

[1]Center for Earth and Planetary Studies, Smithsonian Institution, Washington, D. C., USA.
[2]Hawai'i Institute of Geophysics and Planetology, School of Ocean and Earth Science and Technology, University of Hawai'i at Manoa, Honolulu, Hawaii, USA.
[3]Department of Astronomy, Cornell University, Ithaca, New York, USA.
[4]National Astronomy and Ionosphere Center, Arecibo Observatory, Arecibo, Puerto Rico.

0148-0227/09/2009JE003406$09.00

Table 1. Radar Observation Parameters

Target Name	Date and Start Time (UT)	Target Latitude and Longitude	Subradar Latitude and Longitude	Minimum–Maximum Incidence Angle	Duration (min)
Seren 1	1 May 2006, 1927:00	17° N, 9.1° E	−6.5° N, 6.2° E	20°–33°	18
Seren 4	15 Sep 2006, 1148:00	18° N, 25.3° E	−6.6° N, 7.6° E	23°–39°	22
Apollo 15	16 Sep 2006, 1208:00	26.2° N, 3.6° E	−6.2° N, 7.3° E	26°–40°	22
Seren 3	16 Sep 2006, 1234:00	16° N, 19.9° E	−6.1° N, 7.2° E	18°–31°	10
Vaporum	16 Sep 2006, 1312:00	12° N, 3° E	−6.1° N, 7.0° E	12°–23°	10

glass beads and/or black crystallized beads [*Gaddis et al.*, 2003, 1985; *Weitz et al.*, 1998; *Lucey et al.*, 1986]. The crystallized beads cooled more slowly and were most likely formed in a dense part of the fire fountain [*Weitz et al.*, 1998, 1996]. Orange glasses and crystallized beads were both recovered at the Apollo 17 site; subsequent analysis showed that their composition was consistent with the spectroscopic characteristics of the Taurus-Littrow pyroclastic deposit to the west [*Gaddis et al.*, 1985; *Adams et al.*, 1974].

[5] Radar provides a different way to study the physical properties of the Moon's surface. The radar echo is sensitive to the composition of the surface (through the dielectric constant and loss tangent), to the presence of subsurface scatterers or interfaces, and to the surface roughness. Materials have a complex dielectric constant ($\varepsilon' + i\varepsilon''$) and loss tangent ($\tan\delta = \varepsilon''/\varepsilon'$) that depend on their composition and porosity. The penetration depth, or distance in the subsurface at which the radar power has decreased by e^{-1}, is $L_p = \lambda/(2\pi\sqrt{\varepsilon'}\tan\delta)$. For terrestrial basalt, the values of ε' are typically around 5–9. Fine-grained materials, such as ash, have dielectric constant values around 2–4 [*Campbell and Ulrichs*, 1969]. Loss tangents for terrestrial materials range from 0.001 to 0.1 for volcanic rocks with a range of densities [*Campbell and Ulrichs*, 1969]. The average dielectric constant of the lunar regolith is 2.8, and loss tangents of the lunar highlands range from 0.01 to 0.001 or less [*Carrier et al.*, 1991]. Previous radar observations and laboratory studies have shown that a higher ilmenite ($FeTiO_3$) content corresponds to a higher loss tangent and lower radar backscatter cross sections at 70 cm wavelength [*Carrier et al.*, 1991; *Campbell et al.*, 1997]. Rocks with very low titanium content can have loss tangents as low as 0.0002 [*Olhoeft and Strangeway*, 1975], leading to large radar penetration depths.

[6] Radar images of Mare Serenitatis at 3.8 and 70 cm wavelength were used as a comparison to Apollo orbital data and mapping results [*Thompson et al.*, 1973]. Radar data at 3.8 cm wavelength were used by *Gaddis et al.* [1985] to identify and trace the boundaries of pyroclastic deposits that were not apparent in optical images due to a relatively high albedo. *Zisk et al.* [1974] used 3.8 cm wavelength high-resolution radar images to trace the margins of localized pyroclastic deposits in the floor of Alphonsus crater. Radar images of the Aristarchus plateau at wavelengths of 12.6 and 70 cm reveal buried lava flows and highlight areas of blocky impact ejecta that are not visible in optical images [*Campbell et al.*, 2008; see also *Zisk et al.*, 1977]. Building on these studies, we collected new ground-based radar images, at 12.6 cm wavelength, for the southern Mare Serenitatis and Mare Vaporum regions in order to study the spatial extent and physical properties of the pyroclastics in these areas, and to search for as yet unidentified deposits. We first discuss the observations and provide an introduction to the radar data products. We then discuss general results for all the observed pyroclastics, and show more detailed analyses for each of the individual deposits.

2. Radar Observations and Data Analysis Strategy

[7] The lunar data described here were acquired using the Arecibo 12.6 cm wavelength (S band) radar and the Green Bank Telescope (GBT) in West Virginia. The round-trip time to the moon is ~2.5 s, which is too short to use Arecibo as both transmitter and receiver. We continuously transmit a single circular polarization with Arecibo and receive the echo in both senses of circular polarization at Green Bank. At the distance of the Moon, the 305 m diameter Arecibo telescope produces a beam that is about 2 arc min across at the half-power point at S band, which translates to 230 km at the distance of the Moon. The size of the area that can be imaged for any given observation depends on whether the beam is projected near the subradar point or near the limbs of the Moon. It is generally possible to image an area about 300 × 600 km in size.

[8] For the highest-resolution imaging, we use a coded waveform with a time resolution of 0.1 μs, a code length of 131071, and a 50 min coherent integration to create delay Doppler images with spatial resolutions of ~20 m. This resolution is comparable to some of the Lunar Orbiter, Apollo panoramic camera, and Clementine high-resolution camera images. We use a transmitter power of 100 kW to obtain good signal-to-noise with a small pixel area. The fast sampling required by this setup, and a limited data rate for the sampling instrument, dictates a maximum of two bits per sample for each of the quadrature samples. We refer to this as observing method one; this strategy was used to produce the South Pole and Aristarchus images by *Campbell et al.* [2006] and *Campbell et al.* [2008].

[9] Using a variation of the above technique, we can generate lower-resolution images by using a shorter coherence time of 20 min, again with a time resolution of 0.1 μs, a code length of 131071, and with two bit sampling. We use a lower transmitter power, about 20–60 kW, to avoid strong frequency sidelobes in the processed images. For this method, we spatially average in the range dimension to match the resolution in the Doppler dimension (~60 m) to improve the signal-to-noise. This moderate resolution, low-power method leads to a better calibration of the two circular polarizations than method one. We refer to this observing strategy as method two.

[10] In both methods, the raw data are correlated with the code and mapped to a simple cylindrical lunar coordinate system. Areas outside the beam are discarded, and the data are mosaicked using a correction for the beam shape to link

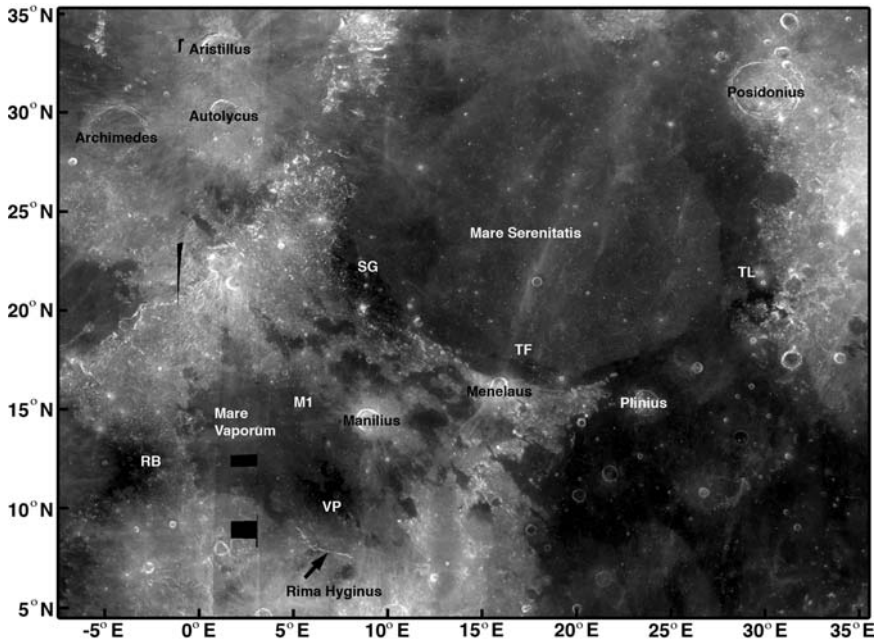

Figure 1. Clementine 750 nm map of the Mare Serenitatis and Mare Vaporum areas with surface features labeled. The map is in a simple cylindrical projection. The locations of the pyroclastic deposits discussed in the text are shown on the map using the following key: RB, Rima Bode; VP, Vaporum; M1, Manilius 1 dome in Mare Vaporum; SG, Sulpicius Gallus; TF, Tacquet Formation; TL, Taurus-Littrow.

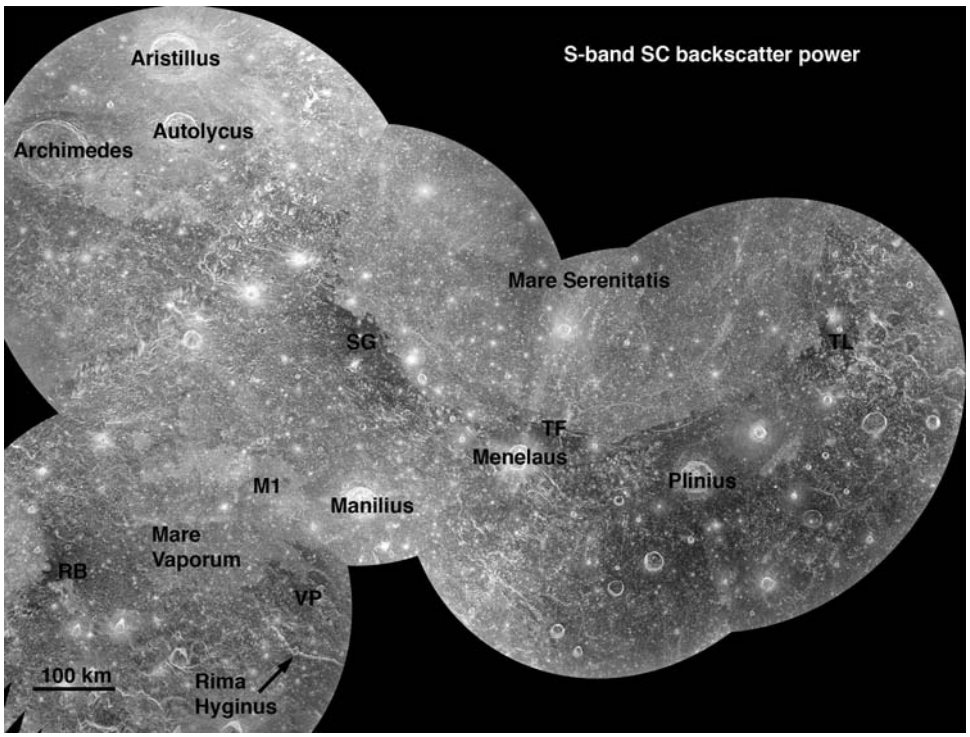

Figure 2. An S band SC (same sense) circular polarization map of Mare Serenitatis and Mare Vaporum, showing the same latitude and longitude range as Figure 1. The map is in a simple cylindrical projection and has been mosaicked using a correction for the antenna beam shape. The data were also normalized using a cosine scattering law. The locations of the pyroclastic deposits discussed in the text are shown on the map using the following key: RB, Rima Bode; VP, Vaporum; M1, Manilius 1 dome in Mare Vaporum; SG, Sulpicius Gallus; TF, Tacquet Formation; TL, Taurus-Littrow.

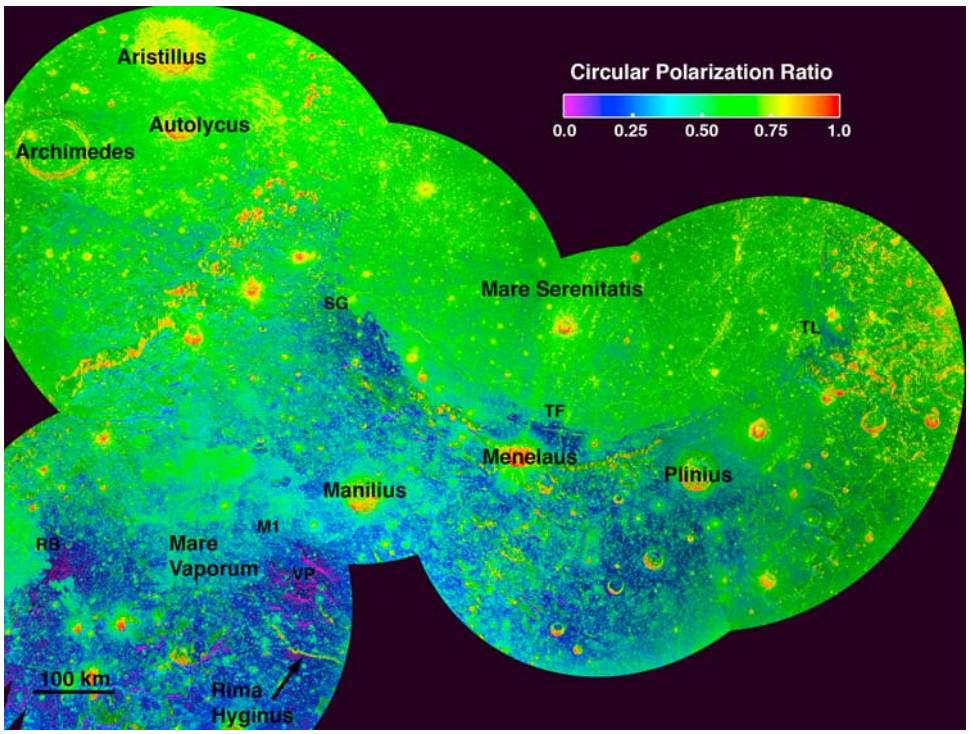

Figure 3. An S band circular polarization map of Mare Serenitatis and Mare Vaporum. The CPR data has been stretched to a color scale and overlaid on the OC image. The map is in a simple cylindrical projection. Large pyroclastic deposits are clearly visible as areas with low CPR values relative to their surroundings. The locations of the pyroclastic deposits are shown on the map using the following key: RB, Rima Bode; VP, Vaporum; M1, Manilius 1 dome in Mare Vaporum; SG, Sulpicius Gallus; TF, Tacquet Formation; TL, Taurus-Littrow.

nearby areas. For the SC image, the data were normalized by the cosine of the incidence angle, but no scattering law normalization was applied to products used to make the circular polarization ration images. We also use data previously obtained at P band (70 cm wavelength) at ~500 m/pixel resolution, as well as a P band image of Mare Serenitatis acquired at 150 m/pixel resolution. The acquisition and processing of the P band data are described by *Campbell et al.* [2007].

[11] The received circular polarization with the opposite sense as the transmitted polarization is abbreviated as OC. At low incidence angles, this power primarily results from mirror-like reflections from radar-facing surfaces that are smooth at the wavelength scale. At higher incidence angles, the OC power is produced by scattering from radar facing slopes as well as by diffuse scattering from wavelength-scale roughness. The same sense circular polarization echo, abbreviated as SC, arises primarily by diffuse scattering from wavelength-sized scatterers on the surface and in the subsurface.

[12] The circular polarization ratio (CPR, or μ_c) can be used as an indicator of surface and subsurface roughness, and is calculated from $\mu_c = \sigma_{sc}/\sigma_{oc}$, where σ_{sc} and σ_{oc} are the backscatter cross sections of the SC and OC data, respectively. Radar echoes from surfaces that are smooth at wavelength scales and that have few embedded wavelength-sized scatterers will have low μ_c values. Diffuse scattering from rough surfaces generates μ_c values approaching one, or even greater than one for extremely rugged terrain such as impact crater ejecta and rough lava flows [*Campbell et al.*, 2006; *Campbell et al.*, 2009].

3. Results and Discussion

3.1. Overview of Pyroclastic Deposits Near Mare Serenitatis and Mare Vaporum

[13] Five separate beam pointings were used to image Mare Serenitatis, Mare Vaporum, and the surrounding pyroclastic deposits (Table 1), using method two (lower resolution) described above. These images were mosaicked together with a resolution of 120 m/pixel. A cosine scattering law was removed from the data. Figure 1 is a Clementine 750 nm image of the observed region, with features labeled for reference. Figure 2 shows the mosaicked SC circular polarization image. The locations of pyroclastic deposits are marked on the image. The corresponding circular polarization ratio values are shown as a color overlay over the OC image in Figure 3. The incidence angle, θ, of the radar waves varies across the map in Figures 2 and 3, depending on the location of the subradar point for each of the five observations (Table 1).

[14] The area shown in Figures 1–3 contains the following pyroclastic deposits, listed from largest to smallest [*Gaddis et al.*, 2003]: Rima Bode, Sulpicius Gallus, Vaporum and Taurus-Littrow. The pyroclastic deposits are generally radar dark in the SC image (Figure 2), most likely because the radar wave can easily penetrate into the fine-grained pyroclastic material and does not encounter as many surface or near-

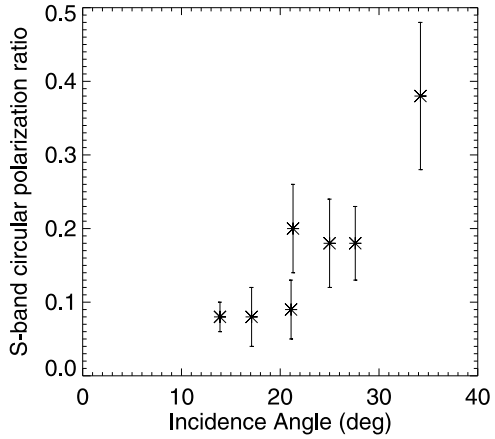

Figure 4. S band circular polarization ratio versus incidence angle for the pyroclastic deposits discussed in the text. Error bars on the μ_c values represent 1 standard deviation. The increase in μ_c with incidence angle is caused by the differing scattering law behaviors for the OC and SC channels. The points shown in the graph represent the following pyroclastic deposits from left to right: Rima Hyginus, Vaporum, Rima Bode, Manilius 1 dome, Tacquet Formation, Sulpicius Gallus, and Taurus-Littrow. The Manilius 1 dome appears to have a larger μ_c value (0.20) relative to other Mare Vaporum area pyroclastics at similar incidence angles, which may indicate a thinner mantling deposit or a higher abundance of surface and subsurface blocks.

surface wavelength-sized blocks as it does in other areas. The radar wave is also sensitive to absorptive minerals, and the data show clear boundaries between low-TiO_2 basalt, which is radar bright, and darker, high-TiO_2 basalt. If individual pyroclastic deposits have a component with a higher loss tangent, it could also contribute to their low-backscatter behavior.

[15] The circular polarization ratio image (Figure 3) can be used to assess surface and near-subsurface roughness. Circular polarization ratio is somewhat dependent on incidence angle because of the shape of the scattering laws; near-nadir scattering is primarily quasi specular and produces mostly OC power and low μ_c values. In Figure 3, the incidence angles and μ_c values thus increase when moving from southwest to northeast (increasing θ) across the image. Figure 4 shows μ_c values versus incidence angle for the individual deposits described below. The error bars in Figure 4 represent one standard deviation. The μ_c values may also have a systematic upward bias of up to a factor of two caused by errors measuring the noise floor in the two bit data. However, measurements across the mosaicked image suggest that the μ_c values of the data set are internally consistent. In the rest of the paper, we use μ_c values to make relative comparisons of terrains at similar incidence angles.

[16] Besides incidence angle effects, a few trends are apparent in the circular polarization ratio data. The pyroclastic deposits typically have very low circular polarization ratios compared to surrounding areas, indicating a general lack of centimeter- to meter-sized surface and subsurface blocks. In some cases, the μ_c values change across individual deposits, suggesting that the amount of surface and embedded blocks also changes across these deposits. For example, the μ_c changes may be caused by contamination from blocky crater ejecta, or by a greater mixing with blocky regolith material as the pyroclastic material thins away from the source. In cases where the original pyroclastic deposit was tens of meters thick, small impactors may not have been able to penetrate through the fine-grained pyroclastics to reach solid rock. Over time, these thicker deposits will continue to have a higher volume of pyroclastics and a lower block abundance than nearby areas. In places where the pyroclastic deposit was originally thin (centimeter to meter), impact gardening will have been able to more thoroughly mix the pyroclastic materials into the regolith, and the μ_c value will more closely match the surrounding areas. Mare areas have high circular polarization ratios, most likely because meteoritic bombardment into solid basalt generates more surface and subsurface blocks than similar impacts into loose material. Crater walls and ejecta blankets have high μ_c values because they have rough surfaces with extensive centimeter- to meter-sized blocks. In sections 3.2–3.7, we discuss individual pyroclastic deposits in and around Mare Serenitatis and Mare Vaporum, moving roughly west to east around each of the mare basins.

3.2. Sulpicius Gallus Pyroclastic

[17] The Sulpicius Gallus pyroclastic deposit mantles both mare and highlands terrain near Rimae Sulpicius Gallus, and is embayed by younger mare basalts. Based on crater depth measurements, *Lucchitta and Schmidt* [1974] estimated that the deposit may be up to 50 m thick. Figure 5 is an expanded view of the μ_c values of the pyroclastic deposit, and Figure 6 is a metric camera image of Rimae Sulpicius Gallus, with the northern outlines of the low μ_c value region drawn in a dashed line. Figure 6 has a different viewing geometry than the radar image and is not mapped to the same coordinate system, but the lighting conditions highlight the regional topography. Around the northern parts of Rimae Sulpicius Gallus, the radar dark and low

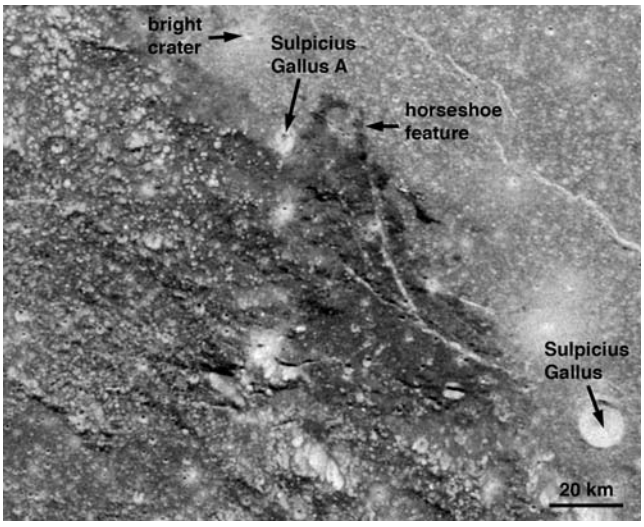

Figure 5. An S band circular polarization ratio image of Sulpicius Gallus with a resolution of 120 m/pixel. North is toward the top. The pyroclastic deposit, including the dark horseshoe-shaped feature, has low circular polarization ratio values.

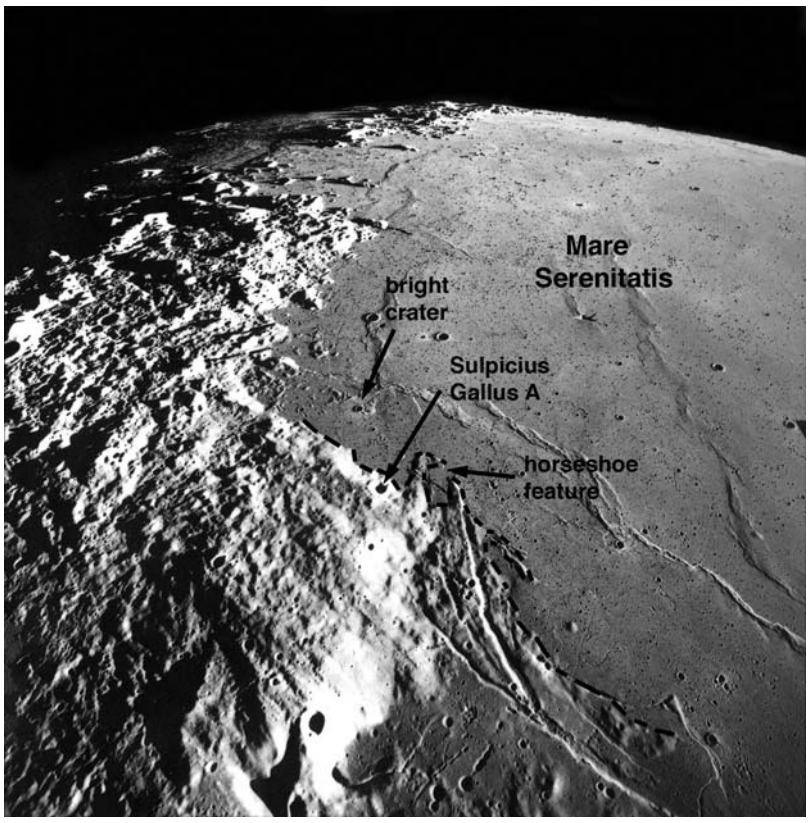

Figure 6. A metric camera image of the Sulpicius Gallus pyroclastic deposit and rille system showing the radar bright crater and horseshoe feature (AS17-M-0953). The image has an oblique viewing geometry that clearly shows the steep slope connecting the elevated highlands to Mare Serenitatis. The boundaries of the pyroclastic deposit as seen by radar (Figure 5) are drawn with a dashed black line. North is toward the top.

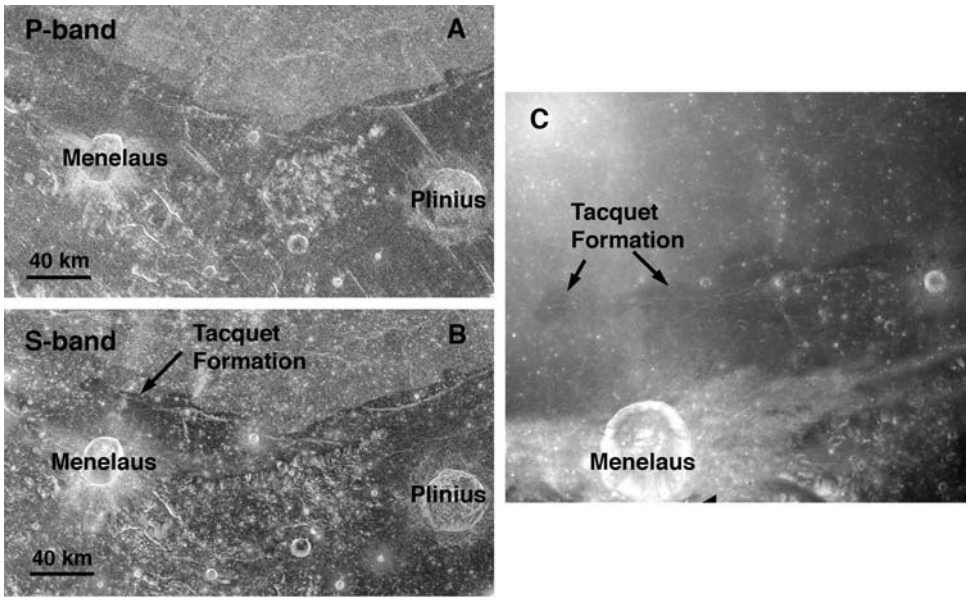

Figure 7. (a) P band (70 cm wavelength) image of the Tacquet Formation with a resolution of 150 m/pixel. (b) S band image of the Tacquet Formation, with a resolution of 120 m/pixel. The S band data shows boundaries between the mare and pyroclastic deposit more clearly. (c) An Apollo metric camera image of the Tacquet Formation (AS15-M-2035). North is toward the top.

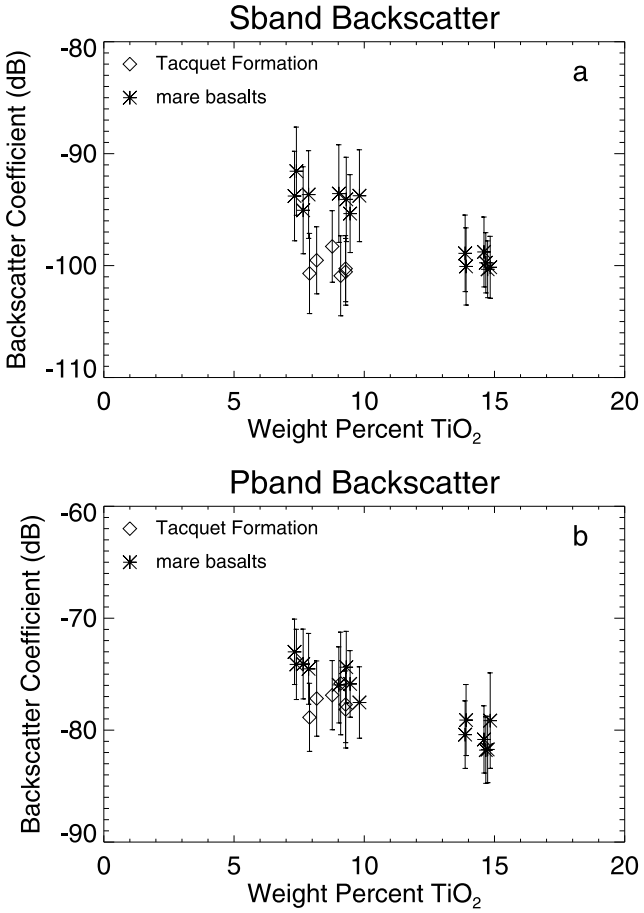

Figure 8. Graphs of Tacquet Formation radar backscatter versus TiO_2 content measured from Clementine data. (a) S band SC (depolarized) backscatter values are significantly below what would be expected for the measured titanium content. (b) P band SC backscatter is slightly less than the backscatter expected for mare basalt with a similar titanium content. In Figures 8a and 8b, backscatter coefficient values are relative to an arbitrary reference level and have not been scaled to a fully calibrated backscatter cross-section value. In Figures 8a and 8b, the error bars show 1 standard deviation of the measured average.

μ_c pyroclastic materials overlie elevated terrain that was not covered by the younger Serenitatis mare basalts.

[18] The portions of the Sulpicius Gallus deposit with the lowest S band radar backscatter lie on the mare in close proximity to the rimae and have μ_c values of 0.18 ± 0.05, compared to the surrounding mare basalt μ_c values of 0.73 ± 0.23. A section of the deposit to the northwest of the crater Sulpicius Gallus A has a higher μ_c value (0.39 ± 0.10) than the main part of the pyroclastic deposit, but still a much lower μ_c value than the Serenitatis mare basalts or the cratered highlands. This portion of the deposit lies on a slope facing away from the incident radar wave (Figure 5), and the higher incidence angles likely contribute to the increase in μ_c. The circular polarization ratio images of this sloping region also show streaks extending downslope, which may indicate either rough, rocky mass wasting deposits along a steep section of the slope, or perhaps a contribution from the rays of a small crater on the nearby mare. There is little immediate change in μ_c when moving from mantled mare areas (e.g., "horseshoe feature") to mantled highland areas, suggesting that the deposit near the rimae was originally fairly thick. Moving southwest into the highlands, the μ_c values gradually approach those of the highland material, which suggests that the deposit was originally thinner toward the southwest.

3.3. Tacquet Formation

[19] The ~2200 km^2 Tacquet Formation in southern Mare Serenitatis appears dark at 750 nm wavelengths, and was mapped by *Carr* [1966] as volcanic flows with a possible component of pyroclastics. The mosaicked data (Figure 3) reveal that the Tacquet Formation has a low radar backscatter cross section and a low circular polarization ratio (0.18 ± 0.06), similar to that of the Sulpicius Gallus deposit to the west. It also has a low-backscatter cross section in the 70 cm data (Figure 7). It is not listed as a pyroclastic deposit by *Gaddis et al.* [2003] or *Weitz et al.* [1998].

[20] Mare basalts with a high TiO_2 content can also be very radar dark [e.g., *Campbell et al.*, 1997], and high-titanium basalt covers the southeast edge of Mare Serenitatis near Plinius. To investigate the effects of titanium on the backscatter values, we measured the SC backscatter at S and P band, along with the TiO_2 content, using the method of *Lucey et al.* [2000], for boxes on the Tacquet Formation and the surrounding maria. In Figure 8, the mare basalt samples sites are negatively correlated with titanium content, as expected from prior work [*Carrier et al.*, 1991; *Campbell et al.*, 1997]. However, at both wavelengths the Tacquet Formation boxes have SC backscatter values that fall below the TiO_2 trend. It is therefore unlikely that the low backscatter of the Tacquet Formation is solely due to a higher titanium content.

[21] The same boxes chosen for the graphs in Figure 8 were used to measure μ_c values. Basalts near the potential pyroclastic deposit have much higher μ_c values (0.40 to 0.66), despite having been imaged at similar incidence angles. A low CPR can also be generated by a smooth, unmantled surface, but none of the surrounding mare areas exhibit similarly low S band μ_c values. The combination of low backscatter and low CPR suggest that the Tacquet Formation is mantled by a fine-grained, block-free pyroclastic deposit. The area of low μ_c corresponds almost exactly with the Tacquet Formation boundaries as mapped by *Carr* [1966].

[22] It is likely that the mantling on the Tacquet Formation is thin. Optical imagery shows subdued terrain, but the features are not muted to the extent that they are at Taurus-Littrow or Sulpicius Gallus. The distinct elongated shape of the deposit, visible in both Clementine 750 nm images and S band radar data, is absent in the P band data, and the P band backscatter values are depressed only 1–2 dB below the expected trend for variations in titanium content. It is possible that the radar sees completely through the pyroclastic material, particularly in the longer-wavelength P band data.

3.4. Taurus-Littrow and the Apollo 17 Landing Site

[23] The Apollo 17 mission landed in the Taurus-Littrow Valley, to the southeast of the Taurus-Littrow pyroclastic deposit. We obtained images of the Taurus-Littrow region at ~30 m/pixel using method one as well as circular polari-

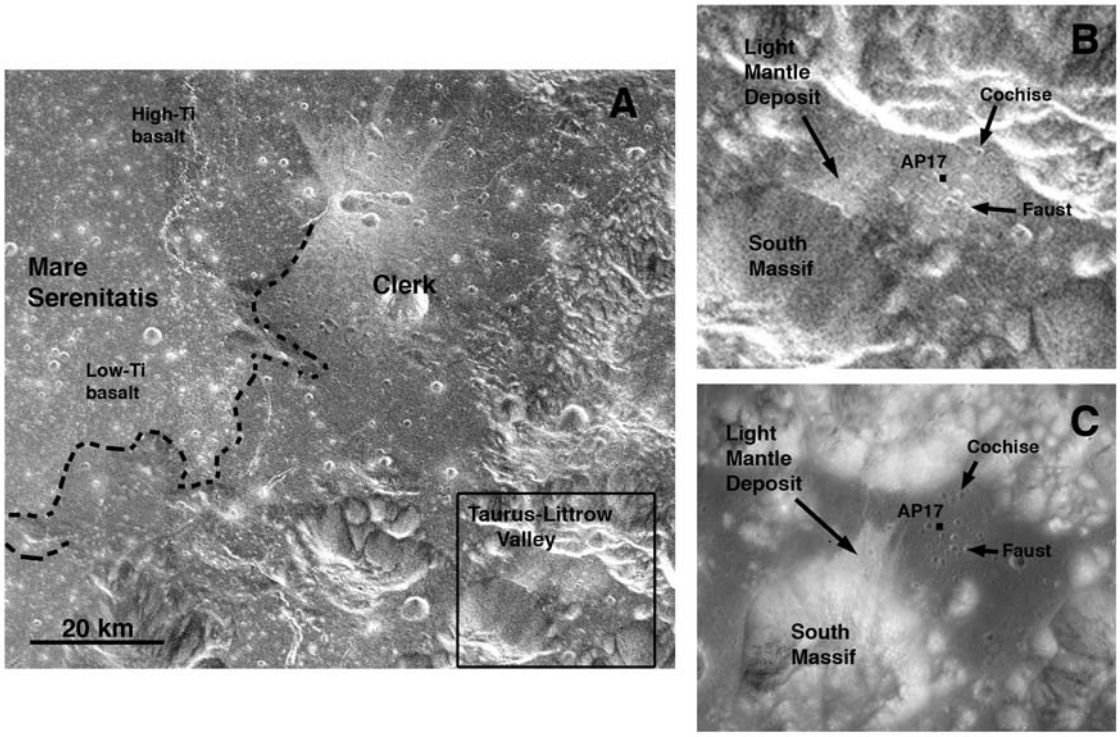

Figure 9. (a) High-resolution (30 m/pixel) S band image of the Taurus-Littrow pyroclastic deposit. The dashed black line is the boundary between the pyroclastic material and unmantled mare basalt as mapped by *Wolfe et al.* [1981]. (b) A subimage showing the Apollo 17 landing site. (c). A metric camera image of the Apollo 17 landing site for reference (AS15-M-0972). The metric camera image has not been converted into a map coordinate frame, but numerous common features are visible in Figures 9b and 9c. A black square marks the location of the Apollo 17 landing site. North is toward the top.

zation ratio values using method two. The average μ_c values for the Taurus-Littrow pyroclastic are significantly higher than those for the western Serenitatis deposits because of the greater incidence angle. The μ_c value for the pyroclastics, measured away from areas with abundant craters, is 0.38 ± 0.10, compared to values of 0.95 ± 0.36 for the mare basalts to the north and west of the deposit.

[24] At high resolution (Figure 9a), the radar dark boundaries of the Taurus-Littrow pyroclastic deposit closely match those mapped by *Wolfe et al.* [1981]. The lowest backscatter and μ_c values occur in the western portion of the deposit, suggesting that the pyroclastic deposit was originally thicker toward the west. In the Taurus-Littrow Valley, small craters visited by the Apollo 17 astronauts are clearly visible (Figures 9b and 9c). These craters, part of an extended Tycho ray [*Weitz et al.*, 1998], are surrounded by radar bright terrain that is presumably due to the decimeter-scale basalt blocks and buried rocky ejecta that surround the secondary craters. The light mantle deposit, which is most likely an avalanche deposit from South Massif [*Howard*, 1973], is also rough and radar bright.

3.5. Rima Bode

[25] The Rima Bode pyroclastic deposit covers primarily highlands terrain on the eastern side of Sinus Aestuum. *Gaddis et al.* [1985] mapped the Rima Bode deposit as two separate areas; a thin deposit covering highlands in the east, and a very dark, thicker, unit in the west that *Gaddis et al.* [1985] label unit A. The radar dark portions of the Rima Bode pyroclastic have an average μ_c value of 0.09 ± 0.04 and closely conform to the deposit seen in optical images and mapped by *Wilhelms* [1968], *Gaddis et al.* [1985], and *Weitz et al.* [1998].

[26] An expanded view of the radar image of the Rima Bode area (Figure 10) shows that the portion of the deposit on the western side near the Sinus Aestuum basalts appears darker to the radar and has a lower μ_c value. The lower μ_c values are indicative of a very rock-poor deposit, suggesting that the pyroclastics are thicker in the southwest portion of the deposit and have mixed with the rocky highlands material in the northern and eastern sections. These thicker western portions correspond to the central part of the *Gaddis et al.* [1985] unit A. The easternmost parts of the deposit do not show a clear boundary with the surrounding highlands, probably because as the mantling deposit thins, the radar backscatter is progressively more influenced by the underlying highland terrain.

3.6. Vaporum and Rima Hyginus

[27] The Vaporum pyroclastic deposit, shown in Figure 11 is draped over lunar highlands in southeastern Mare Vaporum just north of Rima Hyginus. In Figure 11, the dark outline of the northernmost part of the deposit corresponds to a dark boundary in the 750 nm Clementine image (Figure 1). However, the circular polarization ratio image does not show clear boundaries between the pyroclastic deposit and highland and mare materials on the west and south sides. The circular polarization ratio is low compared

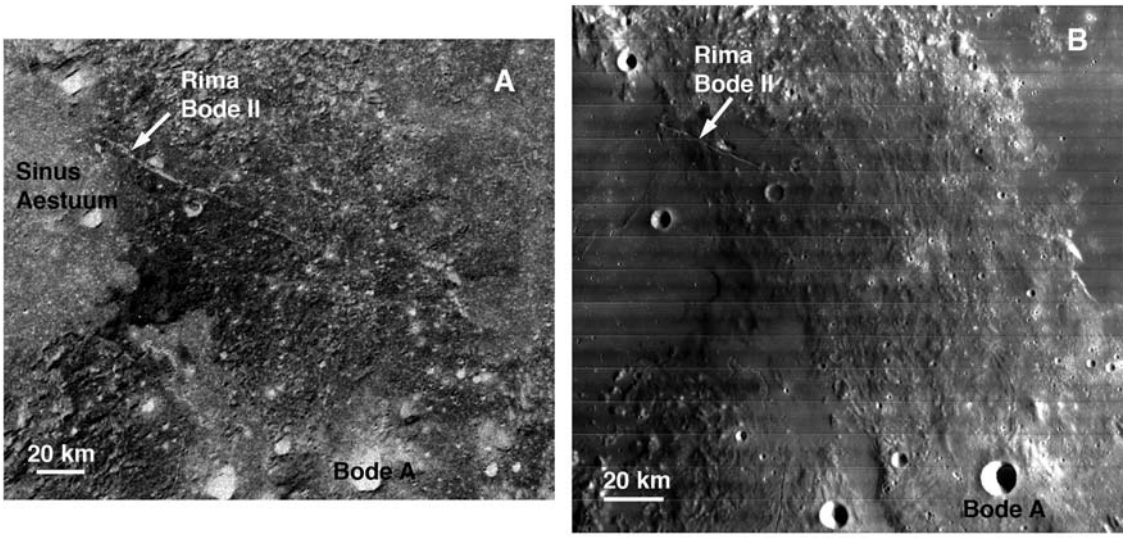

Figure 10. (a) An S band image of the circular polarization ratio values in the vicinity of Rima Bode. The lowest CPR values occur in areas nearest Sinus Aestuum. (b) A Lunar Orbiter 4 image of the Rima Bode pyroclastic (frame 4109). North is toward the top.

to the surroundings, as it is with the previously discussed pyroclastic deposits. The darkest portions of the main deposit as mapped by *Wilhelms* [1968] and *Weitz et al.* [1998] have μ_c values of 0.08 ± 0.04.

[28] Another area of low μ_c values is found near Rima Hyginus, a ~220 km long linear structure south of Mare Vaporum that has a flat floor and numerous pit craters along its length. Small areas with μ_c values of 0.08 ± 0.02 surround the crater Hyginus, which connects two branches of the rille, contains several small hills, and is thought to be volcanic in origin [*Hawke and Coombs*, 1987]. In optical images (Figure 12), Hyginus crater is surrounded by a smooth, dark deposit that has been previously interpreted either as mare basalt [*Wilhelms*, 1968; *Pike*, 1976], or as pyroclastic material [*Hawke and Coombs*, 1987]. Although the dark deposit has slightly elevated TiO_2 values relative to its surroundings (~6% weight percent), the S band SC backscatter values are similar to those of the Vaporum pyroclastic and the Tacquet Formation. As with the Tacquet Formation, it is unlikely that such low S band backscatter values could be produced solely by a mare basalt compositional change. In particular, the low μ_c values surrounding

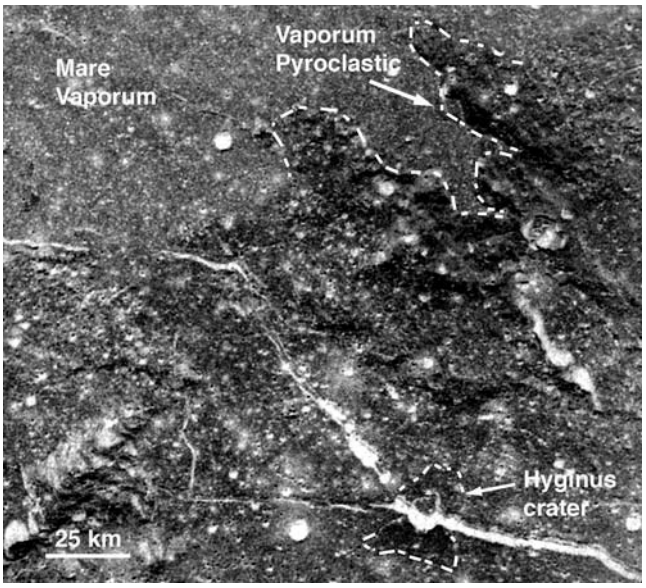

Figure 11. An S band image showing circular polarization values associated with the Vaporum pyrolastic deposit and Hyginus crater dark deposits. Visible boundaries of low CPR value regions are shown with dashed white lines. North is toward the top.

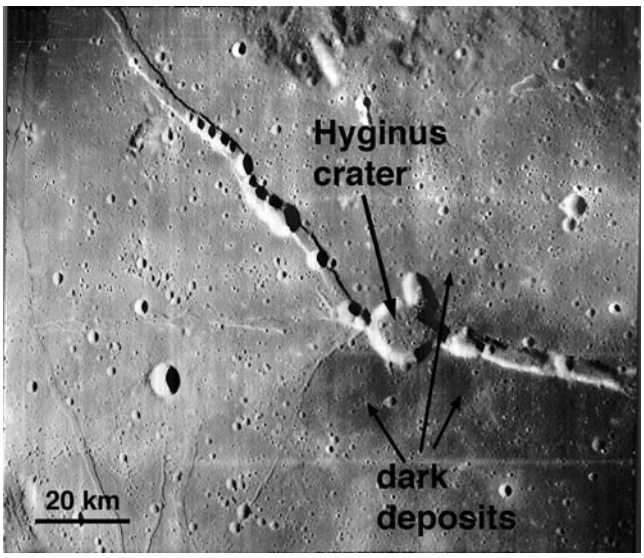

Figure 12. A Lunar Orbiter 5 image (frame 5096) showing the location of dark deposits surrounding Hyginus crater [e.g., *Pike*, 1976]. Hyginus crater is about 11 km across and is located at 7.8° N and 6.3° E. Numerous dome structures can be seen in the crater interior. North is toward the top.

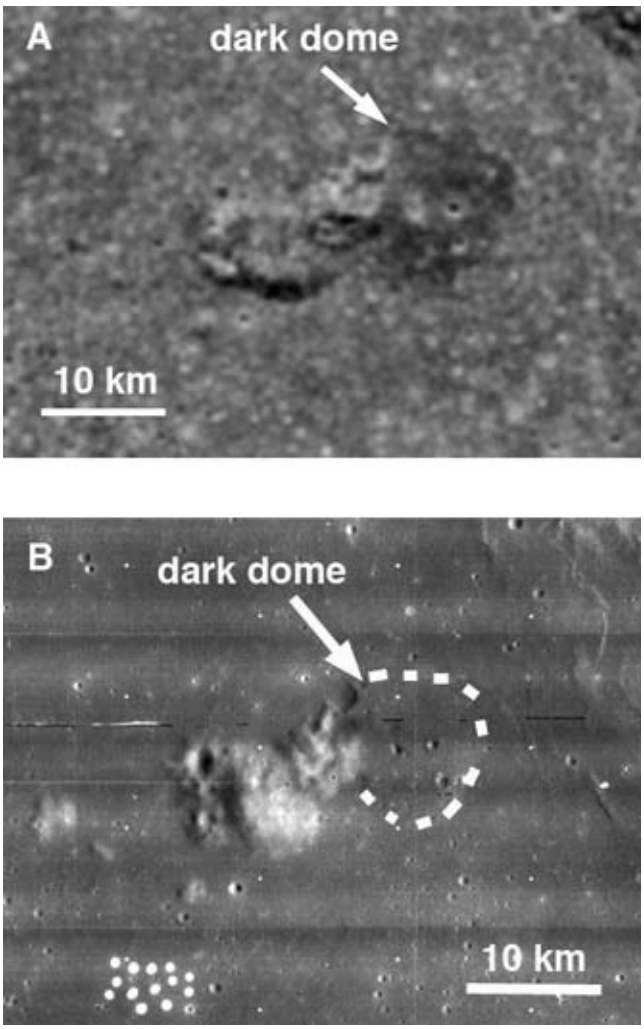

Figure 13. (a) A circular polarization ratio image of the Manilius 1 dome in Mare Vaporum. The dome appears as a dark circle surrounded by mare basalts with higher μ_c values. Bright areas to the west (left side) are peaks extending out of the mare near the dome. (b) A Lunar Orbiter 4 image of the Manilius 1 dome (frame 4102). The boundary between the dome (with the low circular polarization ratio values) and the mare basalts is shown with a white dashed line. In Figures 13a and 13b, north is toward the top.

Hyginus crater are similar to those of the nearby Vaporum pyroclastic deposit, which suggests that fine-grained, rock-poor material such as pyroclastics may also surround Hyginus crater.

3.7. Dome (Manilius 1) in Mare Vaporum

[29] *Wilhelms* [1968] maps numerous hills and domes in central Mare Vaporum as potential volcanic constructs. One of these features, a ~12 km diameter dome located at 15.2 N and 5.8 E and listed as Manilius 1 by *Head and Gifford* [1980], has a μ_c value of 0.20 ± 0.06, significantly below values for the surrounding basalts (μ_c = 0.36 ± 0.09). Figure 13 shows the circular polarization ratio image along with a Lunar Orbiter image. A metric camera image of the dome and its surroundings can be seen in Figure 14. The low, optically dark dome is connected to a small set of peaks to the west. *Head and Gifford* [1980] classify the dome as a circular feature with low slopes and a summit crater (Class 1), and they interpret this and similar domes as volcanic constructs that were most likely formed through extrusive volcanism. These low-relief domes are considerably different in morphology from terrestrial cinder cones, and may be similar to some terrestrial shields formed through Hawaiian or Strombolian eruptions from a central pipe vent or small fissure [*Head and Gifford*, 1980]. In the 70 cm wavelength radar data, the dome has SC backscatter values that are indistinguishable from the surrounding mare basalts, suggesting that any block-poor pyroclastic component to the regolith is thin.

[30] The modeled Clementine titanium abundances show a slight decrease in TiO_2 (<1%) for the dome feature relative to the surrounding mare. Since lower backscatter from mare basalts is linked with higher TiO_2, this low backscatter at S band is unlikely to be the result of variations in the mare basalt composition. The low S band backscatter and low μ_c values suggest that this dome may be covered in fine-grained pyroclastic material that is thin enough to be transparent to the P band wave. The μ_c value for the dome is significantly higher than those of other Mare Vaporum area pyroclastics (Figure 4), which may indicate that the mantling deposit is thinner and partially transparent to the S band wave. Alternatively, the mantling material may have more surface and embedded centimeter-sized blocks than the other nearby pyroclastic deposits.

[31] It is not clear why other domes in the Manilius area do not have low μ_c values, or why the low μ_c values are tightly constrained to the Manilius 1 dome and do not appear to extend onto the nearby hills. It is possible that the dome is older and has been embayed by younger mare basalts that removed any evidence of a broader distribution of pyroclastics. It is also possible that pyroclastic material is largely confined to an area near the central vent; however, in this case it seems unlikely that no trace of mantling material would be visible on the surrounding mare. A thin layer of fine-grained material might be invisible on the nearby hills

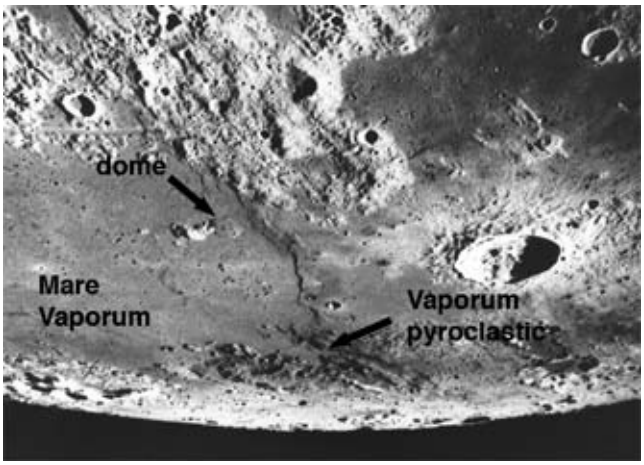

Figure 14. A metric camera image (AS17-M-1672) of the Mare Vaporum area showing the Manilius 1 dome that exhibits low μ_c values. North is at the top of the image.

due to the tendency of material (including any preexisting blocky highland material) to shed downhill, which tends to add surface and subsurface scatterers. In addition, the radar viewing geometry becomes more complex in areas of steep slopes, which adds to the difficulties in comparing μ_c values. Many of the other Manilius area domes listed by *Head and Gifford* [1980] are classified as "Class 6" domes, which have no central vent and may not be of extrusive origin. In cases where the domes appear to have a central vent, but do not have lower μ_c values, the domes may not have associated pyroclastic deposits.

4. Summary and Future Work

[32] The low radar backscatter and μ_c values associated with pyroclastic material provide a useful method of distinguishing fine-grained volcanic material from optically dark maria. In the lunar radar data, the fine-grained pyroclastic deposits appear darker than surrounding terrain, including the radar dark high-titanium basalts. Unlike optical and infrared data, the 12.6 cm wavelength radar data are not sensitive to surface optical albedo and therefore offer a different method of highlighting areas with differing surface and near-subsurface textures. Most of the observed pyroclastic deposits have a stronger backscattered power contrast with the surrounding terrain at the 12.6 cm wavelength than at 70 cm wavelength. Multiwavelength radar data can also be useful for determining which areas of pyroclastic deposits are contaminated by crater ejecta, and which areas are thinner.

[33] Two spacecraft imaging radars are currently orbiting the Moon or planned for future launch – the Forerunner (S band, 13 cm wavelength) instrument on the Indian Space Agency Chandrayaan-1 and the miniRF (X and S band, 4 and 13 cm wavelengths) instrument on NASA's Lunar Reconnaissance Orbiter. These radars will both be capable of full Stokes parameter imaging [*Chin et al.*, 2007] and will be able to generate similar polarization products to those discussed here. These radars will therefore be an excellent method of studying lunar volcanic settings, and may be able to detect pyroclastic deposits in areas where optical images and infrared compositional studies produce ambiguous results.

[34] **Acknowledgments.** We thank the telescope operations staff at Arecibo and the Green Bank Telescope (GBT), especially the transmitter operators Alfredo Santoni, Victor Negrón, and Joe Green. John Chandler at the Harvard-Smithsonian Center for Astrophysics provided lunar ephemeris tables. Two anonymous reviewers provided helpful comments. Arecibo Observatory is part of the National Astronomy and Ionosphere Center, which is operated by Cornell University under a cooperative agreement with the National Science Foundation (NSF). The GBT is part of the National Radio Astronomy Observatory, a facility of the NSF that is operated under cooperative agreement by the Associated Universities, Inc. D.B.C. acknowledges partial support under the NASA Planetary Astronomy program.

References

Adams, J. B., C. Pieters, and T. B. McCord (1974), Orange glass—Evidence for regional deposits of pyroclastic origin on the moon, *Proc. Lunar Planet. Sci. Conf.*, *5*, 171–186.

Campbell, B. A., B. R. Hawke, and T. W. Thompson (1997), Regolith composition and structure in the lunar maria: Results of long-wavelength radar studies, *J. Geophys. Res.*, *102*, 19,307–19,320, doi:10.1029/97JE00858.

Campbell, B. A., D. B. Campbell, J. L. Margot, R. R. Ghent, M. Nolan, J. Chandler, L. M. Carter, and N. J. S. Stacy (2007), Focused 70-cm mapping of the Moon, *IEEE Trans. Geosci. Remote Sens.*, *45*, 4032–4042, doi:10.1109/TGRS.2007.906582.

Campbell, B. A., L. M. Carter, B. R. Hawke, D. B. Campbell, and R. R. Ghent (2008), Volcanic and impact deposits of the Moon's Aristarchus plateau: A new view from earth-based radar images, *Geology*, *36*, 135–138, doi:10.1130/G24310A.1.

Campbell, B. A., B. R. Hawke, and D. B. Campbell (2009), Surface morphology of domes in the Marius hills and Mons Rümker regions of the Moon from Earth-based radar data, *J. Geophys. Res.*, *114*, E01001, doi:10.1029/2008JE003253.

Campbell, D. B., B. A. Campbell, L. M. Carter, J. L. Margot, and N. J. S. Stacy (2006), No evidence for thick deposits of ice at the lunar poles, *Nature*, *443*, 835–837, doi:10.1038/nature05167.

Campbell, M. J., and J. Ulrichs (1969), Electrical properties of rocks and their significance for lunar radar observations, *J. Geophys. Res.*, *74*, 5867–5881, doi:10.1029/JB074i025p05867.

Carr, M. C. (1966), Geologic map of the Mare Serenitatis region of the Moon, *U. S. Geol. Surv. Misc. Geol. Invest. Map, I-489*.

Carrier, W. D., G. R. Ohloeft, and W. Mendell (1991), Physical properties of the lunar surface, in *Lunar Sourcebook: A User's Guide to the Moon*, edited by G. Heiken, D. Vaniman, and B. M. French, pp. 475–567, Cambridge Univ. Press, Cambridge, U. K.

Chin, G., et al. (2007), Lunar Reconnaissance Orbiter overview: The instrument suite and mission, *Space Sci. Rev.*, *129*, 391–419, doi:10.1007/s11214-007-9153-y.

Gaddis, L. R., C. M. Pieters, and B. R. Hawke (1985), Remote sensing of lunar pyroclastic mantling deposits, *Icarus*, *61*, 461–489, doi:10.1016/0019-1035(85)90136-8.

Gaddis, L. R., M. I. Staid, J. A. Tyburczy, B. R. Hawke, and N. E. Petro (2003), Compositional analyses of lunar pyroclastic deposits, *Icarus*, *161*, 262–280, doi:10.1016/S0019-1035(02)00036-2.

Hawke, B. R., and C. R. Coombs (1987), Remote sensing studies of the Rima Hyginus region of the Moon, *Proc. Lunar Planet. Sci. Conf., XVIII*th, 407–408.

Hawke, B. R., C. R. Coombs, L. R. Gaddis, P. G. Lucey, and P. D. Owensby (1989), Remote sensing and geologic studies of localized dark mantle deposits on the moon, *Proc. Lunar Planet. Sci. Conf.*, *XIX*th, 255–268.

Head, J. W., and A. Gifford (1980), Lunar mare domes: Classification and modes of origin, *Earth Moon Planets*, *22*, 235–258, doi:10.1007/BF00898434.

Howard, K. A. (1973), Avalanche mode of motion: Implications from lunar examples, *Science*, *180*, 1052–1055, doi:10.1126/science.180.4090.1052.

Lucchitta, B. K., and H. H. Schmidt (1974), Orange material in the Sulpicius Gallus Formation at the southwestern edge of Mare Serenitatis, *Proc. Lunar Planet. Conf.*, *V*th, 466–467.

Lucey, P. G., B. R. Hawke, T. B. McCord, C. M. Pieters, and J. W. Head (1986), A compositional study of the Aristarchus region of the moon using near-infrared reflectance spectroscopy, *J. Geophys. Res.*, *91*, D344–D354, doi:10.1029/JB091iB04p0D344.

Lucey, P. G., D. T. Blewett, and B. D. Joliff (2000), Lunar iron and titanium abundance algorithms based on final processing of Clementine UV-visible images, *J. Geophys. Res.*, *105*, 20,297–20,305, doi:10.1029/1999JE001117.

Olhoeft, G. R., and D. W. Strangeway (1975), Dielectric properties of the first 100 meters of the Moon, *Earth Planet. Sci. Lett.*, *24*, 394–404, doi:10.1016/0012-821X(75)90146-6.

Pike, R. J. (1976), Geologic map of the Rima Hyginus region of the Moon, *U. S. Geol. Surv. Misc. Geol. Invest. Map, I-945*.

Tera, F., and G. J. Wasserburg (1976), Lunar ball games and other sports, *Proc. Lunar Planet. Sci. Conf.*, *VII*th, 858–860.

Thompson, T. W., K. A. Howard, R. W. Shorthill, G. L. Tyler, S. H. Zisk, E. A. Whitaker, G. G. Schaber, and H. J. Moore (1973), Apollo 17 preliminary science report, *Rep. NASA SP-330*, NASA, Washington, D. C.

Weitz, C. M., J. W. Head III, and D. S. McKay (1996), Eruption and emplacement of lunar pyroclastic glasses as inferred from the 74001/2 section, *Proc. Lunar Planet. Sci. Conf.*, *XXVII*th, 1413–1414.

Weitz, C. M., J. W. Head III, and C. M. Pieters (1998), Lunar regional dark mantle deposits: Geologic, multispectral, and modeling studies, *J. Geophys. Res.*, *103*, 22,725–22,759, doi:10.1029/98JE02027.

Wilhelms, D. E. (1968), Geologic map of the Mare Vaporum Quadrangle of the Moon, *U.S. Geol. Surv. Misc. Geol. Invest. Map, I-548*.

Wilson, L. W., and J. W. Head III (1981), Ascent and eruption of basaltic magma on the Earth and Moon, *J. Geophys. Res.*, *86*, 2971–3001, doi:10.1029/JB086iB04p02971.

Wolfe, E. W., N. G. Bailey, B. K. Lucchitta, W. R. Muelhberger, D. H. Scott, R. L. Sutton, and H. G. Wilshire (1981), Geologic map of the Taurus Littrow area, *U. S. Geol. Surv. Prof. Pap.*, *1080*.

Zisk, S. H., G. H. Pettengill, and G. W. Catuna (1974), High-resolution radar maps of the lunar surface at 3.8-cm wavelength, *Moon*, *10*, 17–50, doi:10.1007/BF00562017.

Zisk, S. H., C. A. Hodges, H. J. Moore, R. W. Shorthill, T. W. Thompson, E. A. Whitaker, and D. E. Williams (1977), The Aristarchus-Harbinger region of the Moon: Surface geology and history from recent remote-sensing observations, *Moon*, *17*, 59–99, doi:10.1007/BF00566853.

B. A. Campbell and L. M. Carter, Center for Earth and Planetary Studies, Smithsonian Institution, P.O. Box 37012, Washington, DC 20013-7012, USA. (carterl@si.edu)

D. B. Campbell, Department of Astronomy, Cornell University, Ithaca, NY 14853, USA.

B. R. Hawke, Hawai'i Institute of Geophysics and Planetology, School of Ocean and Earth Science and Technology, University of Hawai'i at Manoa, POST 602, 1680 East-West Rd., Honolulu, HI 96822, USA.

M. C. Nolan, National Astronomy and Ionosphere Center, Arecibo Observatory, HC03 Box 53995, Arecibo PR00612, Puerto Rico.